AIAA JOURNAL
Vol. 45, No. 12, December 2007

Effectiveness of Dynamically Deflected Tab Control of a Tip Vortex

T. Lee*
McGill University, Montreal, Quebec H3A 2K6, Canada

DOI: 10.2514/1.31426

The control of the tip vortex generated by an oscillating NACA 0015 wing via a dynamically deflected trailing-edge tab, actuated at 29 different start times, amplitudes, and ramp-up rates, was investigated. The upward tab deflection was found to be more effective in weakening the peak tangential velocity and vortex strength than the downward deflection, regardless of the start time and ramp-up rate. A pair of corotating vortices was persistently noticed during pitch-up. An earlier and faster tab deflection (actuated during pitch-up) led to a larger reduction in the core vortex flow quantities. The downward tab deflection was, however, more effective in displacing the vortex position and in diffusing the vortex. The later and slower the downward tab actuation, the larger the vortex displacement and diffusion that took place. The largest reduction in the vortex strength was obtained with a start time at the beginning of pitch-down. The effectiveness of the tab control was also evaluated via the hysteretic behavior of the vortex core flow quantity and the potential suppression of the blade–vortex-interaction noise.

Nomenclature

b	=	semiwing span
C_l	=	section lift coefficient
C_y	=	y_c hysteresis factor, $\int y_c(\alpha)d\alpha$
C_Γ	=	Γ_c hysteresis factor, $\int \Gamma_c(\alpha)d\alpha$
C_θ	=	$v_{\theta\text{peak}}$ hysteresis factor, $\int v_{\theta\text{peak}}(\alpha)d\alpha$
c	=	airfoil chord
d_{miss}	=	vortex–blade miss distance
f	=	oscillation frequency
L	=	blade lift per unit span
l	=	length over which two-dimensional blade–vortex interaction occurs
Re	=	chord Reynolds number, $u_0 c/\nu$
R_1	=	ramp-up rate
R_2	=	ramp-down rate
r	=	radial position
r_c	=	vortex core radius
t_d	=	tab actuation duration
t_s	=	tab actuation start time
t_{ss}	=	steady-state time period
u	=	streamwise velocity
u_o	=	freestream velocity
v_θ	=	tangential velocity
x, y, z	=	streamwise, transverse, and spanwise distances
α	=	angle of attack
$\alpha_m, \alpha_{\max}, \alpha_{\min}$	=	mean, maximum, and minimum α
α_{ss}	=	static-stall angle
α_1	=	α at end of ramp-up motion
α_2	=	α at onset of ramp-down motion
Δ	=	blade–vortex-interaction parameter
$\Delta\alpha$	=	oscillation amplitude
δ	=	deflection amplitude
κ	=	reduced frequency, $\pi f c/u_o$
Γ	=	vortex strength or circulation
Γ_c	=	core circulation
Γ_o	=	total circulation
ζ	=	streamwise vorticity
ν	=	kinematic viscosity
ρ_o	=	freestream fluid density
τ	=	phase angle, $\omega t = 2\pi$ ft

Subscripts

d	=	pitch-down
u	=	pitch-up

I. Introduction

THE tip vortices generated by fixed-wing tips, because of the hazardous effects to any following aircraft that may inadvertently encounter the vortex and the undesired lift-induced drag, continue to be of concern to the aviation industry and aircraft manufacturers alike. For example, Robinson [1] estimated that the current Federal Aviation Administration (FAA) wake–turbulence separations result in a 12% loss in airport capacity when arrivals comprise 50% of the separations. Moreover, tip vortices shed from helicopter rotor blades and propellers interact with following blades, causing rotor noise and vibration. The understanding and control of the tip vortex generated by a finite wing subjected to periodic or unsteady motions is therefore of paramount importance in the reduction of blade–vortex-interaction (BVI) noise and vibration. Extensive experimental investigations have been conducted to characterize the near-field static-wing tip vortices [2–7] and their control. By contrast, a much less vigorous research effort has been devoted to the measurement of the tip-vortex flow behind an oscillating wing. So far, only three refereed experimental investigations [8–10], to the author's knowledge, have been reported. It is noteworthy that measurements of the wake of a hovering rotor have also been made, for example, by Leishman [11], Mahaligam and Komerath [12], and Heineck et al. [13].

The unsteady velocity and vorticity fields associated with a tip vortex in the near field behind an oscillating wing was explored first in detail by Ramaprian and Zheng [8] by using a three-component laser Doppler anemometer. They reported that for a NACA 0015 rectangular wing oscillated with $\alpha(t) = 10\,\text{deg} + 5\,\text{deg}\sin\omega t$ at a reduced frequency $\kappa = 0.1$ and $Re = 1.8 \times 10^5$, the trajectory of the oscillating tip vortex for $0.16 < x/c < 2.66$ was very nearly the same as for a static wing at the mean incidence, where x is the streamwise distance downstream of the wing trailing edge. Also, the normalized circulation distribution across most of the inner part of the vortex for $x/c > 0.7$ exhibited the same universal behavior as the vortex behind a static wing. Chang and Park [9] examined the hysteretic behavior of

Received 5 April 2007; revision received 15 August 2007; accepted for publication 15 August 2007.

*Associate Professor, Department of Mechanical Engineering.

the vortical wake behind a NACA 0012 airfoil oscillated with $\alpha(t) = 15\,\text{deg} + 5\,\text{deg}\sin\omega t$ at $\kappa = 0.09$ for $Re = 3.4 \times 10^4$ by using a triple hot-film probe at $x/c = 0.5$ and 1.5. The peak tangential velocity, the core circulation, and the axial velocity deficit were found to be smaller during pitch-down than during pitch-up. Recently, the details of the near-field vortex flow generated by a NACA 0105 wing subjected to both deep and light stall and attached-flow oscillations at different reduced frequencies for $Re = 1.86 \times 10^5$ was reported by Birch and Lee [10]. Their measurements showed that for attached-flow and light-stall oscillations, there was a small hysteretic property over an oscillation cycle and that many of the vortex flow features were found to be qualitatively similar to those of a static wing. For deep-stall oscillations, a large discrepancy in the magnitude of the critical vortex flow quantities, however, was exhibited between the pitch-up and pitch-down motion. The vortex size was larger during pitch-down than during pitch-up. Moreover, the normalized circulation within the inner region of the oscillating-wing tip vortex also exhibited a self-similar structure, similar to that of a static wing, and was insensitive to the reduced frequency. The magnitude of the critical vortex flow quantities was also found to remain largely streamwise-invariant for $0.75 < x/c < 4$.

In the meantime, a number of passive control schemes [14–17] have been attempted to alleviate the BVI strength by modifying the blade-tip geometry, including the addition of winglets, spoiler, and stub/subwing at the rotor tip or by blowing air along the vortex axis. Hardin and Lamkin [18] suggested theoretically that the severity of the BVI-induced acoustic pressure time history $p(x,t)$ be proportional to $\Gamma l L/\rho_o d_{\text{miss}}^2$. One promising BVI noise-reduction concept is thus to decrease the tip-vortex strength Γ (generated by an unsteady wing) and/or to increase the miss distance d_{miss} at the blade–vortex encounters. Active approaches such as higher harmonic control [19,20], individual blade control [21], and trailing-edge tabs [22–24] have therefore been considered. Among them, the active trailing-edge tab control has been attempted rigorously to achieve a desired reduction in vortex strength and an increase in blade–vortex separation distance. Enenkl et al. [23] tested a full-scale helicopter rotor blade system, incorporated with an active tab control mechanism, and concluded that the BVI noise and vibration can be significantly reduced. The details of the vortex flow characteristics, however, were not reported. Recently, the control of the tip vortex via a prescheduled dynamically deflecting tab, superimposed on a sinusoidally oscillated NACA 0015 wing, was investigated by Panagakos and Lee [24]. The tab actuation employed a brief pulse (represented by a constant ramp-up motion, remained steady briefly, and was followed by a constant ramp-down motion) actuated at two different actuation start times (i.e., $t_s = -0.5$ and 0.167π) and deflection amplitudes ($\delta = 5.3$ and -5.3 deg). Their limited measurements indicated that the downward tab deflection was most effective in displacing the vortex position, whereas upward tab motion was more effective in reducing the peak tangential velocity and vortex strength. A more extensive study of the effects of the tab motion parameters (including the actuation start time, deflection amplitude, and, especially, the tab deflection ramp rate) on the critical vortex flow quantities is needed.

The objective of this study was to extend the previous work of Panagakos and Lee [24] to investigate the various tab motion parameters on the critical vortex flow quantities via a newly integrated tab control system with improved controllability. A parametric study was conducted that had as parameters the start time (between $\alpha_{\min}$ and $\alpha_{\max}$ during pitch-up), deflection duration t_d (50% of an oscillation cycle), ratio of steady-state deflection to total deflection (0% and 50%), ramp-up tab deflection rate R_1 (chosen based on the t_{ss}/t_d and the limits of the mechanical system), and deflection amplitude. A total of 29 tab motion profiles (including five different t_s, five R_1, and two δ, while keeping the ramp-down tab deflection rate R_2 constant) were tested. Special emphasis was placed on the characterization of the effects of different tab motion parameters on the phase-averaged strength, size, shape, and trajectory of the tip vortex over one cycle of oscillation. These measurements were then used to determine a best possible tab deflection motion based upon the desired effects on the various performance characteristics. The hysteretic behavior of the vortical wake for both upward and downward tab motions was also evaluated. Potential alleviation of the blade–vortex-interaction severity was also discussed.

II. Experimental Methods

The experiment was conducted in the newly constructed suction-type wind tunnel in the Department of Mechanical Engineering at McGill University with a freestream turbulence intensity of 0.03% at $u_o = 14.2$ m/s. A square-tipped untwisted NACA 0015 wing with $c = 20.3$ cm and $b = 49.5$ cm, oscillated through the static-stall angle ($\alpha_{ss} = 16.5\,\text{deg}$) with $\alpha(t) = 14\,\text{deg} + 8\,\text{deg}\sin\omega t$ and $\kappa = 0.09$, was used as the test model. The oscillating wing was chosen to simulate the quasi-periodic first-harmonic angle-of-attack variations that are found on helicopter rotors during low-speed forward flight [8,10]. The origin of the coordinate was located at the leading edge of the wing. A specially designed four-bar linkage and flywheel oscillation mechanism (driven by an Exlar model DXM340C servomotor driven by an Emerson model FX3161 PCM1 programmable motion controller) mounted externally on the wind tunnel was used in the present experiment. The oscillation frequency was monitored in real time using an HP model 3581A spectral analyzer and was measured to an accuracy of ± 0.02 Hz. The four-bar mechanism provided an output that was sinusoidal to within 2%. The airfoil pitch axis was located at the quarter-chord location. The instantaneous angle of attack of the airfoil and the phase reference signal τ were recorded from both the servomotor feedback resolver and a potentiometer mounted on the wing shaft. Note that when the phase angle was within the range of $-0.5\pi \le \tau \le 0.5\pi$, the wing was described to be in pitch-up; within $0.5\pi \le \tau \le 1.5\pi$, the wing was said to be in pitch-down. The freestream velocity u_o was fixed at 13 m/s, which rendered a chord Reynolds number of 1.7×10^5.

The wing model was also equipped with a moveable trailing-edge tab (of a chord of 25%c and a span of 13%b), which was activated and deactivated independently by a Maxon servomotor (model Re-35), incorporating a 4.3:1 helical gearbox and an optical encoder (Fig. 1a). The tab was located at the trailing edge, centered at the 93.5%-span position. The tab motion triggered in response to the oscillating-wing phase angle employed a brief pulse and could be

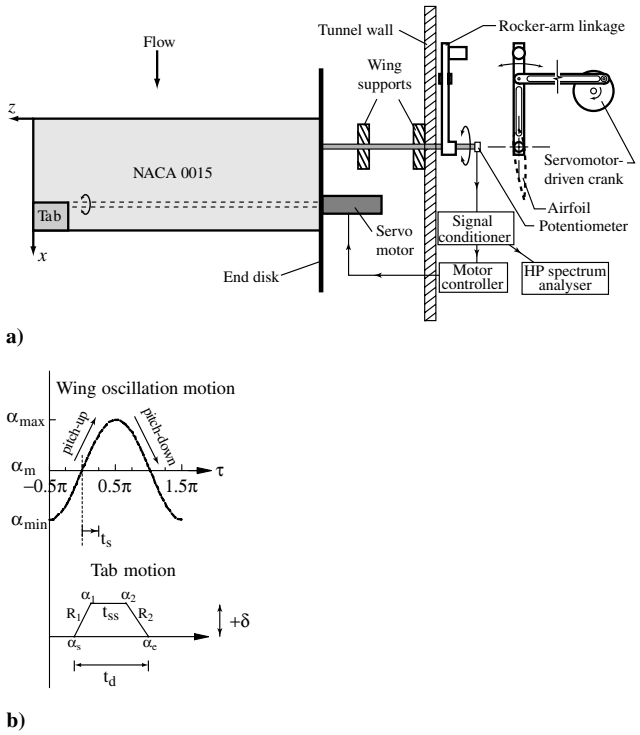

Fig. 1 Illustrations of the a) wing model and b) tab motion parameters.

Table 1 Values of tab motion parameters

Case	δ	R_1	t_{ss}	α_s	α_1	α_e	Case	δ	R_1	t_{ss}	α_s	α_1	α_e
			$t_s = -0.5\pi$							$t_s = -0.5\pi$			
1	+8 deg	5%	35%	6_u	6.4_u	22_u	16	−8 deg	5%	35%	6_u	6.4_u	22_u
2	+8 deg	20%	20%	6_u	11.5_u	22_u				$t_s = -0.25\pi$			
3	+8 deg	40%	0%	6_u	20.5_u	22_u	17	−8 deg	5%	35%	7.8_u	10.4_u	19.6_d
			$t_s = -0.25\pi$				18	−8 deg	10%	30%	7.8_u	12.7_u	19.6_d
4	+8 deg	5%	35%	7.8_u	10.4_u	19.6_d	19	−8 deg	20%	20%	7.8_u	17.7_u	19.6_d
5	+8 deg	10%	30%	7.8_u	12.7_u	19.6_d	20	−8 deg	30%	10%	7.8_u	21.1_u	19.6_d
6	+8 deg	20%	20%	7.8_u	17.7_u	19.6_d	21	−8 deg	40%	0%	7.8_u	21.9_d	19.6_d
7	+8 deg	30%	10%	7.8_u	21.1_u	19.6_d				$t_s = 0\pi$			
8	+8 deg	40%	0%	7.8_u	21.9_d	19.6_d	22	−8 deg	5%	35%	14_u	16.5_u	14_d
			$t_s = 0\pi$				23	−8 deg	10%	30%	14_u	18.7_u	14_d
9	+8 deg	5%	35%	14_u	16.5_u	14_d	24	−8 deg	20%	20%	14_u	21.6_u	14_d
10	+8 deg	10%	30%	14_u	18.7_u	14_d	25	−8 deg	30%	10%	14_u	21.6_d	14_d
11	+8 deg	20%	20%	14_u	21.6_u	14_d	26	−8 deg	40%	0%	14_u	18.7_d	14_d
12	+8 deg	30%	10%	14_u	21.6_d	14_d				$t_s = 0.175\pi$			
13	+8 deg	40%	0%	14_u	18.7_d	14_d	27	−8 deg	5%	35%	17.5_u	20.1_u	9.8_d
			$t_s = 0.175\pi$				28	−8 deg	20%	20%	17.5_u	21.8_d	9.8_d
14	+8 deg	5%	35%	17.5_u	20.1_u	9.8_d				$t_s = 0.5\pi$			
15	+8 deg	20%	20%	17.5_u	21.8_d	9.8_d	29	−8 deg	5%	35%	22_d	21.6_d	6_d

actuated at any desired time t_s or angle of attack α_s. The pulse signal was represented by a constant ramp-up motion, remained steady briefly, and was followed by a constant ramp-down motion (Fig. 1b). The time required to deflect the tab varied between cycles by less than $0.5\%f^{-1}$. The time of tab initial deflection (i.e., start time t_s), the upward ramp rate R_1, deflection amplitude δ, steady-state motion t_{ss}, downward ramp rate R_2, and total deflection time t_d was controlled by a Maxon EPOS 70/10 programmable motion controller. In the present experiment, a total of 29 different tab motion profiles with $t_s = -0.5, -0.25, 0, 0.175$, and $+0.5\pi$ (corresponding to $\alpha_u = \alpha_{\min}$, 8.3 deg, α_m, 18.2 deg, and $\alpha_{\max}$, respectively), δ (+8 deg upward and −8 deg downward or equal to $\pm\Delta\alpha$), and $R_1 = 5$, 10, 20, 30, and $40\%f^{-1}$ were tested. The deflection of $\delta = \pm 8$-deg rendered a maximum upward tab deflection height of about $\pm 3.5\%c$. The actuation duration t_d and R_2 were fixed at 50 and $10\%f^{-1}$, respectively, throughout the test. No reference to R_2 is made because the downward slope of the tab deflection, in general, occurs during the downstroke of the wing oscillation, except for the $t_s = -0.5\pi$ tab control case, when there are no significant events occurring over the wing. As such, the time allocated to the downward tab motion is of secondary importance, in that it was determined as a result of first setting the values of R_1 and t_{ss}. The parameters describing the tab actuation profile in various units are given in Table 1.

The instantaneous velocities were subsequently ensemble averaged over 40–80 oscillating cycles to obtain phased-locked averages of the vortex flow properties at various phase positions during the cycle. A miniature triple hot-wire probe (Auspex Model AVEP-3-102 with a measurement volume of 0.5 mm^3) was used to measure the mean and fluctuating velocity components in planes perpendicular to the freestream velocity at $x/c = 3.0$. The triple hot-wire probe was calibrated in situ, following the calibration procedures described by Chow et al. [5], before the installation of the model. The hot-wire signals were sampled at 500 Hz and were recorded on a PC through a 16-bit A/D converter board. Probe traversing was achieved through a custom-built computer-controlled traversing system. The data plane taken in the near field of the wing model had 56×56 measuring grid points with an increment of $\Delta y = \Delta z = 1.6$ mm (or $0.8\%c$). The maximum experimental uncertainties in the results reported have been estimated as follows [25]: mean velocity 3.5%, vorticity component 8%, vortex radius 4%, and velocity fluctuation 3%. It is also of importance to note that it is known that the magnitude of the critical vortex flow quantities (in particular, the turbulence structure value) is inevitably under the influence of vortex meandering. Fortunately, in the near field and rollup region, it is reported by Devenport et al. [4] that the rms amplitude of the meandering was generally less than $0.5\%c$ and led to a maximum 5 and 6% vortex-meandering-induced variation in the core radius and the peak tangential velocity, respectively. Ramaprian and Zheng [6] further suggested that the effects of vortex meandering only gain significance in the far field. Nevertheless, in the present study, the vortex meandering was examined by using the correlation technique/criteria employed by Chow et al. [5]. The vortex meandering was found to be very small and should not contribute noticeably to the present measurements.

III. Results and Discussion

A. Baseline Wing

To better understand the influence of the prescheduled tab motion on the tip vortex, the characteristic unsteady boundary layer and the transient dynamic-stall vortex (DSV) events developed on a NACA 0015 wing (with no tip effects), oscillated with $\alpha(t) = 14\text{ deg} + 8\text{ deg}\sin\omega t$ at $\kappa = 0.09$, are briefly discussed first (Fig. 2). The critical aerodynamic flow features were extracted from the dynamic C_l loop in combination with the multiple hot-film-sensor on-surface measurements [26] (not shown here). For light-stall oscillations, the onset and end of flow reversal and its sudden breakdown, and the presence of a 2-D DSV were denoted by points 2 to 4 and points 4 to 5 (covering $\alpha_u = 21$ deg to $\alpha_{\max}$), respectively. From $\alpha_{\min}$ to $\alpha_u \approx \alpha_{ss}$ (points 1 to 2), the flow remained attached to the wing upper surface and was characterized by a linear increase in C_l with α. By contrast, the formation of a 2-D DSV and its premature spillage (points 5 to 6) from the wing upper surface were characterized by a sudden rise and drop in C_l. Beyond point 6 (or $\alpha_d \approx 20$ deg), the pitch-down flow reattachment began and persisted for the rest of the oscillation cycle. Also shown in Fig. 2 are the static C_l-α curves; a static-stall angle of 15 deg (compared with a dynamic-stall angle of around 22 deg) and 16.5 deg was observed for a static wing without and with free end effects, respectively.

Figure 2 also shows that in comparison with the variation of C_l with α during pitch-up, the Γ_o value (indicative of the bound circulation and thus C_l) was also found to increase continuously with α in a rather linear manner, all the way up to $\alpha_{\max}$ (i.e., points 1 to 5) but to a reduced extent. During the during-stall and poststall flow processes (i.e., from points 5 to 6 and 6 to 7, respectively), the reduction in Γ_o was also found to have a much lesser extent compared with the corresponding dynamic C_l value at the same α and, subsequently a reduced Γ_o hysteresis. The circulation, or vortex strength, was obtained by summing the vorticity multiplied with the incremental area of the measuring grid. Also, because of the convection time required for a tip-vortex flow structure to propagate from the wing to the downstream location of the sensor, there is a phase lag between any instantaneous sensor reading and the position of the wing at that instant. In the present experiment, the phase lag was corrected by employing the phase-lag compensation scheme suggested by Chang and Park [9].

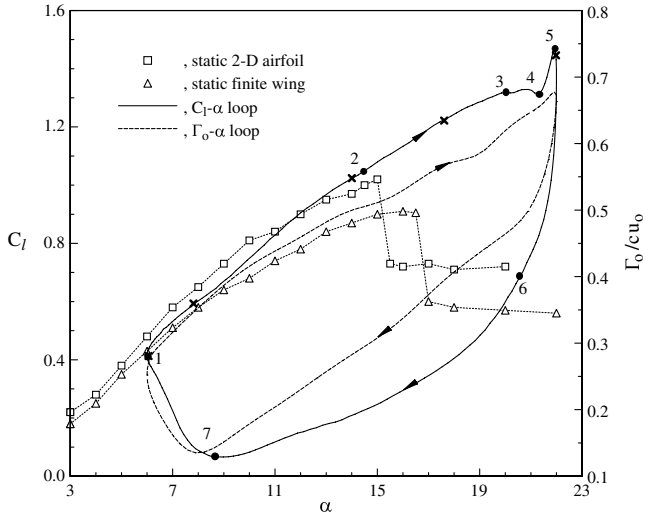

Fig. 2 Baseline wing C_l-α and Γ_o-α curves; filled circles denote the critical unsteady boundary layer and dynamic stall events, and × symbols denote the start of tab actuation.

B. Effect of R_1

The impact of ramp-up rate R_1 (5, 10, 20, 30, and 40% of the oscillation cycle) of the tab motion on the tip-vortex flow was investigated first by setting $t_s = -0.25\pi$ and $\delta = 8$ deg and is presented in Figs. 3–7. This t_s value was chosen to ensure that the tab deflection began during the attached-flow regime (i.e., at $\alpha_u = 7.8$ deg). The representative overall behavior of the tip vortex under the influence of the tab motion can be illustrated by the normalized isovorticity contours presented in Figs. 3a–3d for $R_1 = 10\% f^{-1}$. This particular R_1 value, coupled with $t_s = -0.25\pi$, translates into an upward tab deflection actuated at $\alpha_u = 7.8$ deg, completed its ramp-up motion by $\alpha_u = 11$ deg, began ramp-down motion at $\alpha_u = 21.9$ deg, and ended the deflection by $\alpha_d = 17$ deg. Figures 3a and 3b show that one of the most pronounced phenomena of upward tab control was the presence of a tab vortex, formed at the inboard or inner edge of the tab, in addition to the tip vortex. This tab vortex was corotating with the tip vortex and had a considerably weaker strength compared with the tip vortex at the same angle of attack. The tab vortex was persistently exhibited during the pitch-up motion of the oscillating wing and was found to be pushed downward (below the wing trailing edge) and further inboard by the stronger tip vortex. The tip vortex was always displaced above and inboard of the baseline wing tip (Figs. 3d–3f), regardless of the magnitudes of R_1 and t_s, by the upward tab motion. Note that the tab vortex was also found to continue to orbit the tip vortex as it progressed downstream and would eventually merge with the tip vortex to form a single vortex. After stall, the double vortex was no longer observed (Fig. 3c), due to the fact that the tab was embedded in a DSV-induced separated-flow region. It is of interest to note that the strength of the tab vortex greatly decreased with increasing R_1 for all the t_s tested in the present experiment. That is, the larger the R_1 or the slower the ramp-up rate, the weaker the strength of the tab vortex. For $R_1 > 30\% f^{-1}$, the tab vortex was, however, noticed to be of negligible strength compared with the tip vortex (Fig. 3h). In summary, it can be seen that

1) Upward tab deflection always led to the presence of a double vortex during pitch-up.

2) The tab vortex was of significantly smaller size and strength compared with the tip vortex.

3) The strength of the tab vortex decreased rapidly with increasing R_1 and became insignificant for $R_1 > 30\% f^{-1}$.

The influence of the tab motion on the tip vortex was also discussed in a quantitative way, in terms of the changes in the critical vortex flow quantities (Fig. 4). Note that for cases (i.e., at $\alpha_u \geq 18$ deg) in which the vortex was irregularly shaped, the critical vortex flow quantities were circumferentially averaged values.

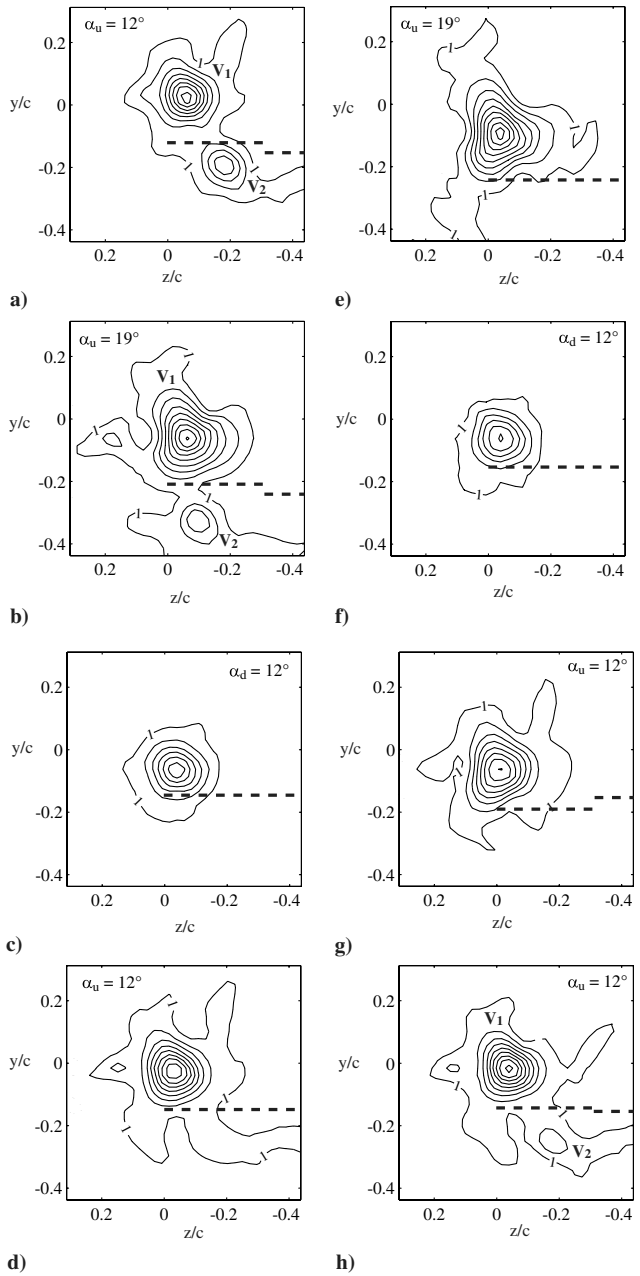

Fig. 3 Representative normalized isovorticity contours with a constant increment of 2; dashed lines denote the wing's trailing edge: a)–c) $\delta = +8$ deg, $t_s = -0.25\pi$, and $R_1 = 10\% f^{-1}$; d–f) baseline wing; g) $\delta = -8$ deg, $t_s = -0.25\pi$, and $R_1 = 10\% f^{-1}$; and h) $\delta = +8$ deg, $t_s = -0.25\pi$, and $R_1 = 40\% f^{-1}$; V1 is the tip vortex and V2 is the tab vortex.

Figures 4a–4e show that the upward tab deflection always led to a tip vortex of weakened peak tangential velocity $v_{\theta\text{peak}}$ and vorticity ζ_{peak}, accompanied by a smaller core radius r_c and core circulation Γ_c and Γ_o, to a various extent, compared with the baseline wing. The observed reduction in ζ_{peak}, Γ_c, and Γ_o was originated from the effective negative camber effects, especially in the trailing edge of the wing, and the unloading of the tip region by the upward tab deflection. The tab upward deflection also created a weakened pressure on both sides (i.e., lower and upper) of the tab. As such, the crossflow over the tip of the tab decreased and thus there presented a drop in the tangential velocity. The extent of the suppression of the critical tip-vortex flow quantities was found to be a strong function of R_1. The smaller the R_1 (or the faster the tab ramp-up motion), the smaller the $v_{\theta\text{peak}}$, ζ_{peak}, r_c, Γ_c, and Γ_o, regardless of t_s, observed. This favorable reduction was due to the fact that the faster the tab

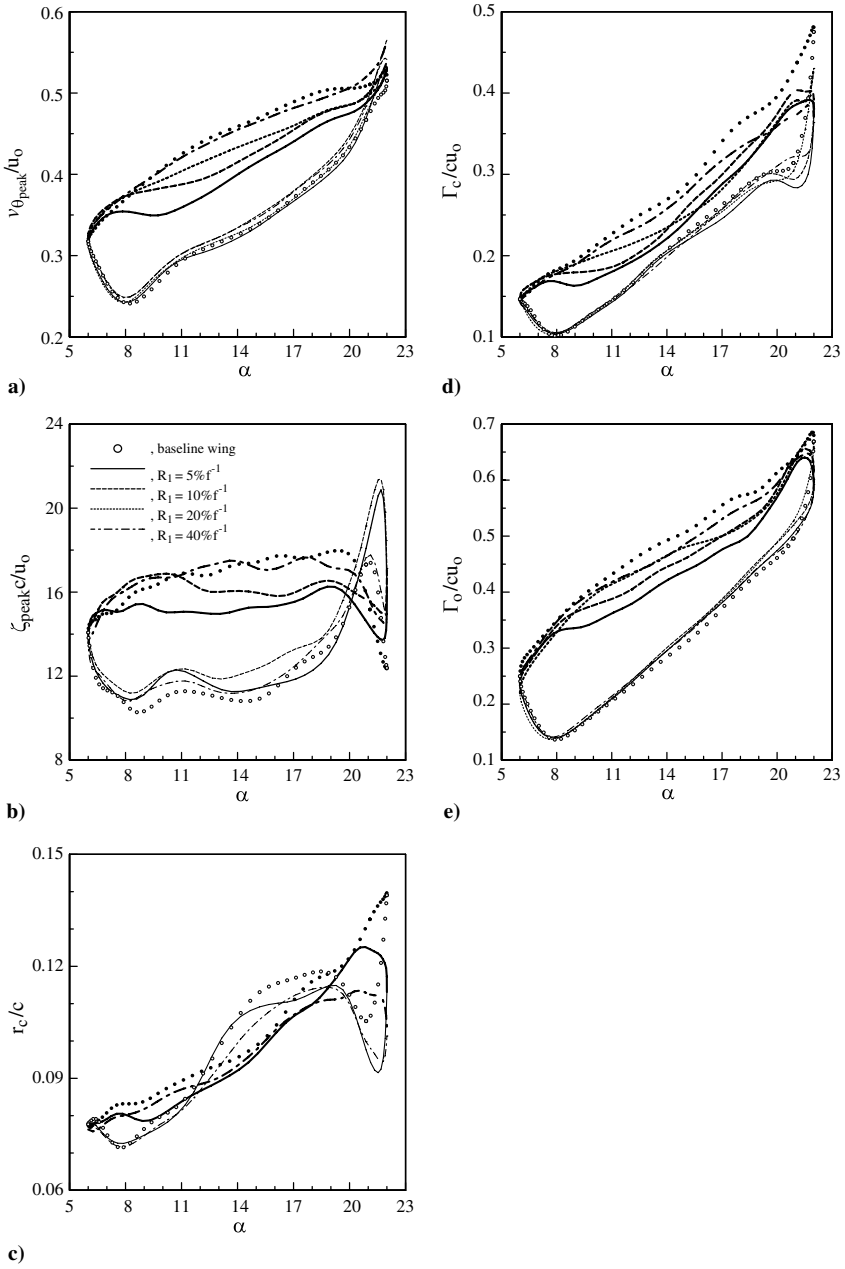

Fig. 4 Effects of R_1 on critical vortex flow quantities for $t_s = -0.25\pi$ and $\delta = +8$ deg.

deflected, the larger the tab deflection angle was during the pitch-up attached-flow condition (and thus a lower value and ensuing weaker tip vortex), which is similar to the effect that reducing the start time had (as discussed later in Sec. III.C). The present measurements also show that no significant influence on the tip-vortex flow was obtained during pitch-down, regardless of R_1 and t_s tested. A reduction of 13, 13, 17, and 16% in $v_{\theta\text{peak}}$, ζ_{peak}, Γ_c, and Γ_o, respectively, for example, at $\alpha_u = 15$ deg was observed for the $R_1 = 5\%f^{-1}$ control case. Details of the influence of the tab motion on the tip-vortex flow can be better depicted from the distributions of v_θ and ζ across the vortex center along the z axis at $\alpha_u = 12.2$ and 19.2 deg during pitch-up (Fig. 5). The reduction in the rotational speed (Fig. 5a) and ζ (Fig. 5b) with decreasing R_1 was evident in comparison with the baseline wing at the same instantaneous angle of attack. In summary, the tab control with $R_1 = 5\%f^{-1}$ produced the most pronounced reduction in the critical vortex flow quantities. The slower deployment of the tab (for example, the $R_1 = 40\%f^{-1}$ control case), however, seems to be the least effective one and rendered no significant change in the tip-vortex flow.

The effects of R_1 on the vortex position for $t_s = -0.25\pi$ and $\delta = +8$ deg were also examined and are displayed in Fig. 6. Figures 6a and 6b show that in addition to the observed reduction in $v_{\theta\text{peak}}$, ζ_{peak}, r_c, and Γ_c, the upward tab deflection also led to a noticeable vertical shifting of the position y_c of the vortex center (taken as the location of ζ_{peak}) above and inboard of the baseline wing to various levels, depending on the magnitudes of R_1. A smaller R_1 rendered a larger y_c displacement. The vertical displacement of y_c during pitch-up also translates into an increased d^2_{miss} (as suggested by Hardin and Lamkin [18]) and presumably a less severe BVI. Note that in the present measurement, the y_c value always referred to the wing trailing edge at zero angle of attack and thus sometimes presented a negative value. Additionally, the tab motion was found to be more effective in displacing the vortex in the vertical direction than in the horizontal direction. As for the tab vortex, due to its interaction with the stronger tip vortex, it was pushed further outboard and down (or below the baseline wing; Figs. 6c and 6d). The y_c and z_c displacement of the tab vortex was, however, found to be independent of the magnitude of R_1.

The effectiveness of the tab control of the tip vortex can also be evaluated by looking into the hysteretic behavior of the vortex core flow quantities, in terms of C_θ, C_Γ, and C_y, at different R_1 and t_s (Fig. 7). The hysteresis factors C_θ, C_Γ, and C_y are defined as the line

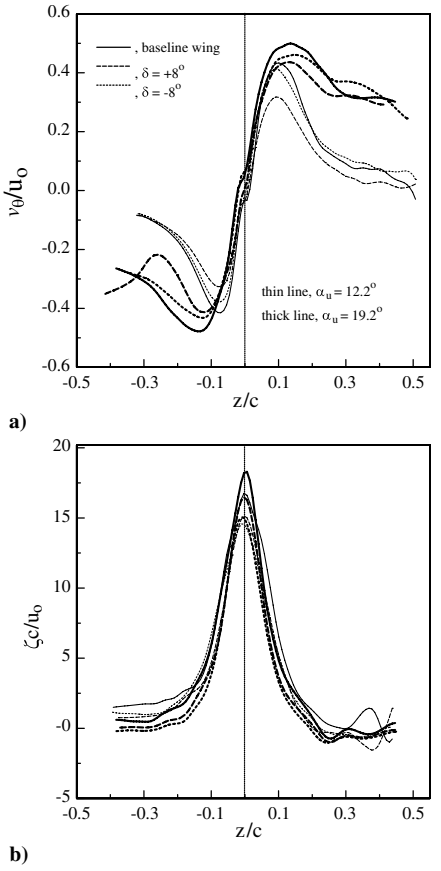

Fig. 5 Typical v_θ and ζ distributions across the vortex center along the z axis for $t_s = -0.25\pi$.

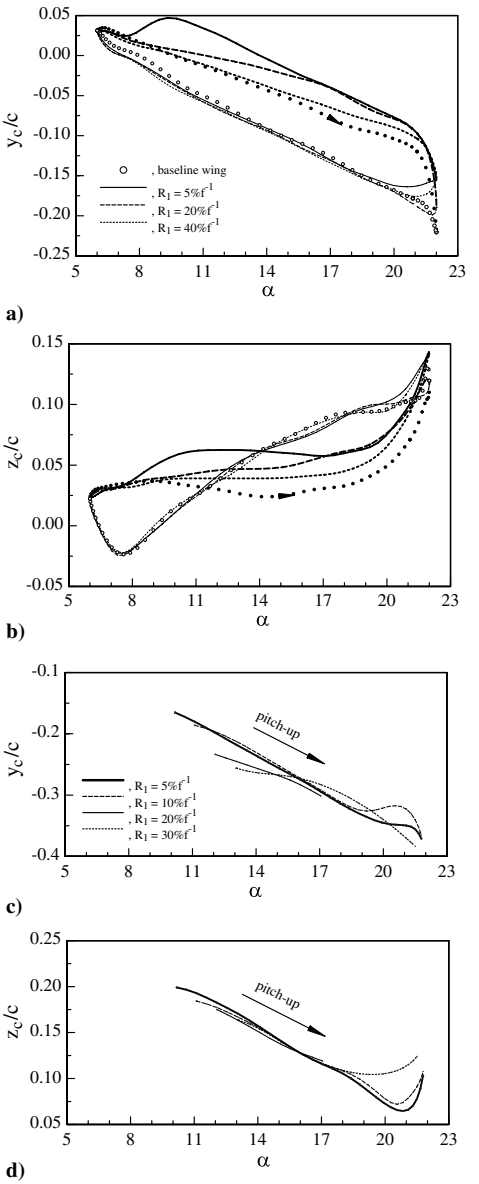

Fig. 6 Variation of the vortex position with R_1 for $t_s = -0.25\pi$ and $\delta = +8$ deg: a–b) tip vortex and c–d) tab vortex.

integrals of the $v_{\theta\text{peak}}$, Γ_c, and y_c versus α curves, respectively, over one oscillation cycle. Figures 7a and 7b show that for $t_s = -0.25\pi$ and $\delta = +8$ deg, the hysteresis in $v_{\theta\text{peak}}$ and Γ_c loops was improved and became smaller than the baseline-wing value and was increased with increasing R_1. The C_y value was, however, observed to increase above the baseline-wing data (an indication of increased d^2_{miss}) and was decreased with increasing R_1. It is clear from Figs. 7a–7c that for a tab deflection actuated at $t_s = -0.25\pi$, the $R_1 = 5\%f^{-1}$ control case produced the most effective control of the tip vortex. The effects of upward tab deflection actuated at a later time during pitch-up (i.e., at $t_s = 0\pi$) on the hysteretic behavior of the vortex core flow were also included in Figs. 7a–7c. The C_θ was still smaller than the baseline wing but had a value much larger than the $t_s = -0.25\pi$ control case. In the meantime, the C_Γ factor was found to remain close to that of the baseline wing. Moreover, a minor improvement in C_y compared with the baseline wing was also observed. The results clearly support the previous findings that an earlier tab actuation during pitch-up gave an enhanced improvement in the vortex core flow compared with tab motion actuated at a later time. It is of importance to note that depending on the value of t_s, a reduction of local lift (induced by the upward tab deflection) during pitch-up would contribute to a decrease in various hysteresis factors, whereas during pitch-down the contribution would be positive. It is, therefore, the proportion of tab deflection duration during pitch-up to that during pitch-down that determines whether the hysteresis increases, decreases, or remains roughly unchanged.

C. Effect of t_s

As stated in Sec. III.B, the faster the ramp-up rate, the more favorable a suppression of the vortex flow achieved. In this section, the effects of the tab actuation start time t_s (-0.5, -0.25, 0, and 0.175π, corresponding to an upward tab actuation started between $\alpha_{\min}$ and 18.2 deg during pitch-up) on the tip vortex with R_1 fixed at $5\%f^{-1}$ are summarized in Figs. 7–9. Figures 8a–8c show that an earlier tab deflection (actuated during pitch-up) generally resulted in a larger reduction in the magnitudes of $v_{\theta\text{peak}}$, r_c, and Γ_c. The $t_s = -0.5\pi$ control case, however, was found to generate the largest reduction in the critical vortex flow quantities. Note that for tab deflection lasting through $\alpha_{\max}$ (i.e., with $t_s = -0.25$, 0, and 0.175π control cases), a considerable reduction in the vortex core flow quantities during the poststall flow condition was also exhibited. In the meantime, the vortex was displaced further vertically above and inboard of the baseline wing with decreasing t_s during the extent of tab deflection (Fig. 8d). The earlier upward tab actuation, the larger the vortex displacement. Note also the significant upward movement of the vortex position during pitch-down for the $t_s = 0.175\pi$ control case. In summary, an earlier and faster upward tab actuation was very effective in alleviating the strength of a tip vortex or, equivalently, d^2_{miss} via enhanced vortex diffusion with a weakened rotational speed. The effectiveness of t_s on the tip-vortex control was also evaluated based on the hysteresis associated with the various vortex core flow quantities (Figs. 7d–7f).

Figures 7d and 7e show that the magnitudes of C_θ and C_Γ were always below that of the baseline wing (except for the $t_s = 0.175\pi$ control case) and were increased, in a rather linear manner, with increasing t_s. That is, the earlier the tab actuation during pitch-up, the larger the reduction or improvement in extent or degree of $v_{\theta\text{peak}}$ and

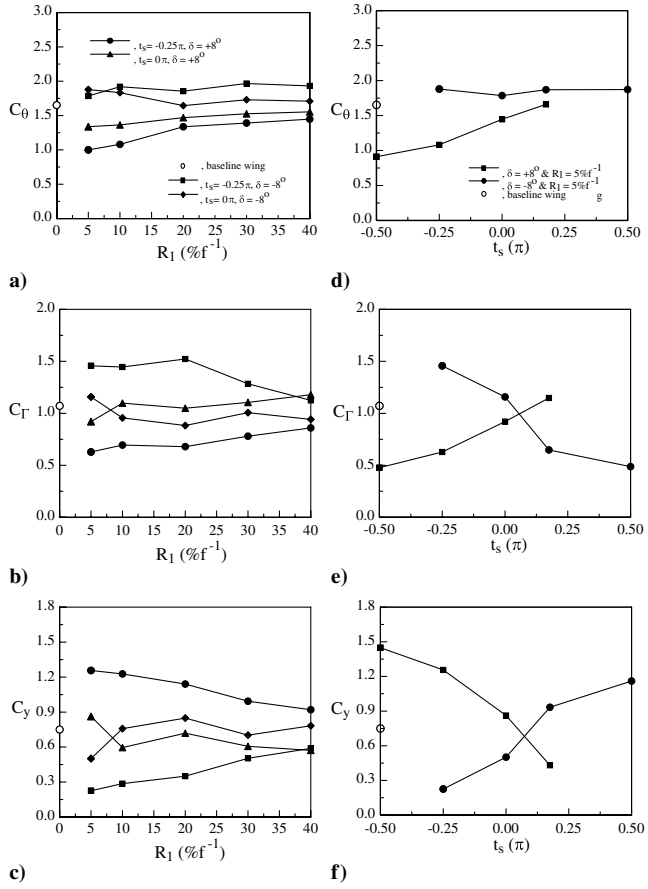

Fig. 7 Hysteretic behavior.

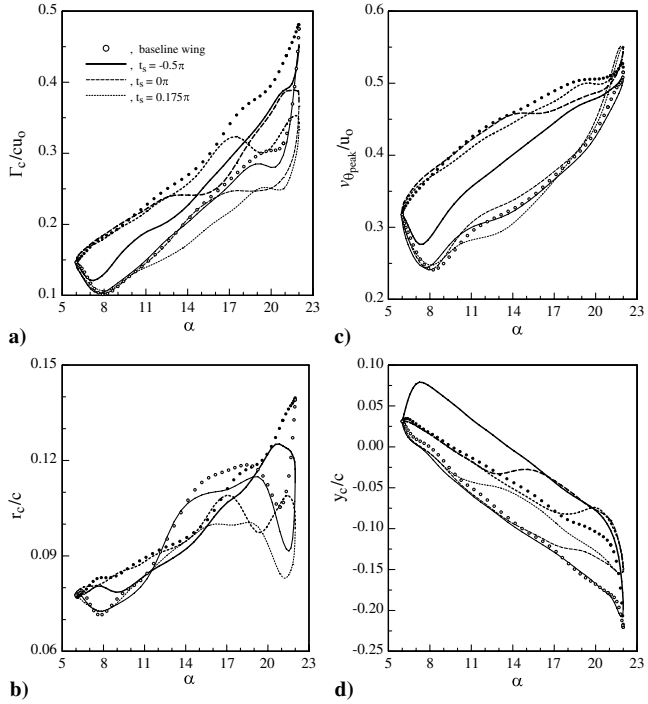

Fig. 8 Effect of t_s on vortex core flow quantities for $\delta = +8$ deg and $R_1 = 5\%f^{-1}$; thick line is pitch-up and thin line is pitch-down.

Γ_c hysteresis achieved. The C_y value was, however, found to decrease with increasing t_s, suggesting that the vortex was displaced closer to the baseline wing because the tab deflection occurred later (Fig. 7f). The results also indicate that for $t_s \geq 0.175\pi$, the values of C_θ and C_Γ were found to rise slightly above the baseline-wing value, and the C_y value fell below the baseline-wing data. This further suggests a benefit from earlier start times with faster ramp-up rates. The observed increase and decrease trend in C_θ, C_Γ, and C_y, respectively, with t_s is similar to those observed for R_1 (Figs. 7a–7c), but was of higher growth or decay rate.

Finally, the present measurements of y_c and Γ_c on the potential alleviation of the BVI severity were also examined. An estimator

$$\Delta = \frac{\Gamma_c c}{(y_c + c)^2 u_o}\Big|_{\text{controlled}} - \frac{\Gamma_c c}{(y_c + c)^2 u_o}\Big|_{\text{uncontrolled}}$$

following the theoretic expression of Hardin and Lamkin [18], which is equal to the difference between the nondimensional magnitudes of Γ/d_{miss}^2 between a tip vortex with and without tab control, was used to evaluate the effectiveness of tab control of the BVI strength. Figure 9 shows that a consistently improved BVI effect (with $\Delta < 0$) compared with the baseline wing was observed for the control case with $t_s = -0.5\pi$, $R_1 = 5\%f^{-1}$, and $\delta = +8$ deg during the entire pitch-up and during-stall flow processes. The largest reduction in $|\Delta|$ (or, equivalently, the largest BVI suppression) of as much as 18% compared with the baseline wing was obtained at $\alpha_u = 7.8$ deg (i.e., at the beginning of the upward tab deflection) with $R_1 = 5\%f^{-1}$. No significant variation in Δ was, however, observed during the poststall pitch-down flow regime. The present results also indicate that the improvement in Δ became less obvious with increasing t_s and R_1.

D. Effect of δ

The effects of downward tab deflection (with $\delta = -8$ deg) on the tip vortex at different R_1 and t_s were also examined and are presented in Figs. 3, 5, 7, 9, and 10. In contrast to the presence of a double vortex during pitch-up for $\delta = +8$-deg deflection, only a single tip vortex was present for downward tab deflection (Fig. 3g), regardless of R_1 and t_s considered. The size and strength of the tip vortex was found to be always increased during tab actuation (Figs. 10a and 10b), whereas the $v_{\theta\text{peak}}$ was decreased (Fig. 10c), compared with the baseline wing, regardless of t_s. The observed increase in Γ_c during pitch-up (with $t_s < +0.5\pi$) and pitch-down (with $t_s = +0.5\pi$) was due to the downward tab-induced positive camber effects and the delay of DSV detachment, respectively. For the downward tab control with R_1 fixed at $5\%f^{-1}$, an improvement in C_Γ against the baseline wing was observed for $t_s > 0\pi$ (Fig. 7e). That is, the later the downward tab actuation, the smaller the Γ_c hysteresis. Also, as indicated in Figs. 10a–10c, because the peak tangential velocity was found to be affected by t_s in a manner similar to those of r_c and Γ_c but to a much less extent, no significant variation in C_θ with t_s was therefore observed (Fig. 7d). The corresponding variation in the y_c position of the vortex with t_s was displayed in Figs. 7f and 10d. As shown in Fig. 10d, the vortex was shifted further downward below and inboard of the baseline wing with increasing t_s for downward tab deflection. The y_c hysteresis, or C_y factor, was consequently found to be increased with later tab actuation (Fig. 7f). Note that the variation of the critical vortex flow quantities with R_1 at different t_s for $\delta = -8$ deg was also examined and is summarized in Figs. 7a–7c. The results show that regardless of t_s, the magnitudes of C_Γ and C_y seem to decrease and increase, respectively, with increasing R_1, whereas the C_θ was less insensitive to the change in R_1. It can, therefore, be concluded that for a downward tab deflection, a larger R_1 (or a slower tab deflection rate) with a later tab actuation led to an increased reduction in the critical vortex flow quantities as well as an increased downward vortex displacement. Finally, the potential alleviation of the BVI strength by downward tab deflection was also examined and was compared with the upward deflection (Fig. 9). The magnitude of the Δ parameter was of a much larger value for the $\delta = -8$-deg control case compared with the $\delta = +8$-deg case over the entire oscillation cycle, suggesting that downward tab control was less effective than the upward tab control. Note also that no BVI suppression was obtained during pitch-down for the $\delta = -8$-deg control case.

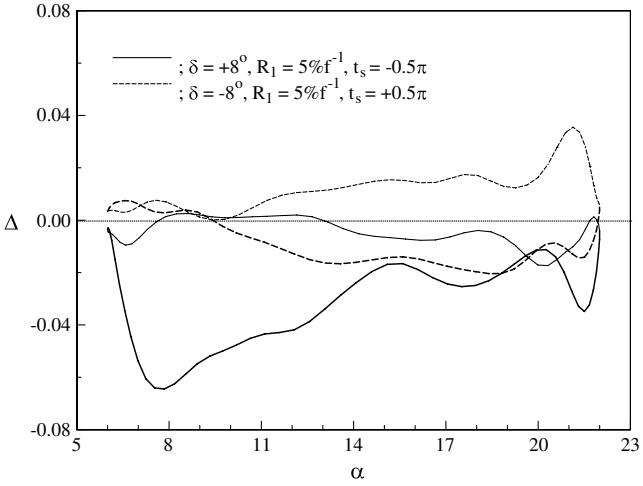

Fig. 9 Typical variation of the Δ parameter with tab motion; thick line is pitch-up and thin line is pitch-down.

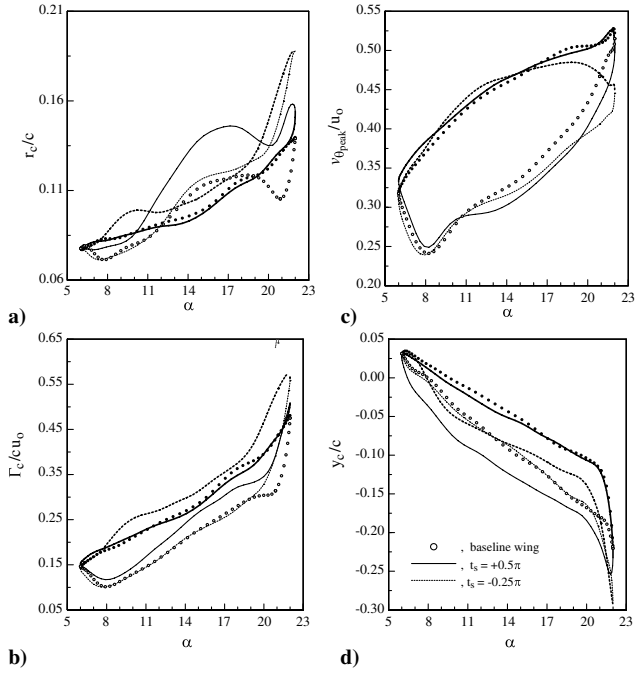

Fig. 10 Variation of vortex core flow quantities with t_s for $\delta = -8\,\mathrm{deg}$ and $R_1 = 5\%f^{-1}$.

IV. Conclusions

A systematic study of the control of the tip vortex generated by an oscillating wing equipped with a dynamically deflecting trailing-edge tab was performed. The upward tab motions were found to be more effective in diffusing the tip vortex and in reducing the peak tangential velocity and vortex strength compared with the downward deflection. A pair of corotating vortices was persistently noticed during pitch-up. The vortex was also found to be displaced further above and inboard of the baseline wing with decreasing t_s and R_1. The faster and earlier upward tab deflection (actuated during pitch-up) achieved a better tab control effectiveness. On the other hand, the downward tab deflection was found to be most effective in displacing the vortex position. The later the actuation and the slower the ramp-up rate, the larger the vortex displacement and vortex diffusion took place. A slower ramp rate actuated at the beginning of pitch-down produced the largest reduction in the vortex strength. The downward tab control was, however, found to be less effective than the upward tab deflection in terms of the potential suppression of the hysteresis associated with the vortex core flow quantities and also the BVI severity.

Acknowledgments

This work was supported by the Natural Science and Engineering Research Council (NSERC) of Canada. P. Gerontakos and J. Pereira are thanked for their help with the experiment.

References

[1] Robinson, J. J., "A Simulation-Based Study of the Impact of Aircraft Wake Turbulence Weight Categories on Airport Capacity," AGARD, CP-584, 1996, pp. 1–15.

[2] Francis, M. S., and Kennedy, D. A., "Formation of a Trailing Vortex," *Journal of Aircraft*, Vol. 16, No. 3, 1979, pp. 148–154.

[3] Green, S. I., and Acosta, A. J., "Unsteady Flow in Trailing Vortices," *Journal of Fluid Mechanics*, Vol. 227, 1991, pp. 107–134. doi:10.1017/S0022112091000058

[4] Devenport, W. J., Rife, M. C., Liapis, S. I., and Follin, G. J., "The Structure and Development of a Wing-Tip Vortex," *Journal of Fluid Mechanics*, Vol. 312, 1996, pp. 67–106. doi:10.1017/S0022112096001929

[5] Chow, J. S., Zilliac, G. G., and Bradshaw, P., "Mean and Turbulence Measurements in the Near Field of a Wingtip Vortex," *AIAA Journal*, Vol. 35, No. 10, 1997, pp. 1561–1567.

[6] Ramaprian, B. R., and Zheng, Y., "Measurements in Rollup Region of the Tip Vortex from a Rectangular Wing," *AIAA Journal*, Vol. 35, No. 2, 1997, pp. 1837–1843.

[7] Birch, D., and Lee, T., "Structure and Induced Drag of a Tip Vortex," *Journal of Aircraft*, Vol. 41, No. 5, 2004, pp. 1138–1145.

[8] Ramaprian, B. R., and Zheng, Y., "Near Field of the Tip Vortex Behind an Oscillating Rectangular Wing," *AIAA Journal*, Vol. 36, No. 7, 1998, pp. 1263–1269.

[9] Chang, J. W., and Park, S. O., "Measurement in the Tip Vortex Roll-Up Region of an Oscillating Wing," *AIAA Journal*, Vol. 38, No. 6, 2000, pp. 1092–1095.

[10] Birch, D., and Lee, T., "Investigation of the Near-Field Tip Vortex Behind an Oscillating Wing," *Journal of Fluid Mechanics*, Vol. 544, 2005, pp. 201–241. doi:10.1017/S0022112005006804

[11] Leishman, J. G., "Measurements of the Aperiodic Wake of a Hovering Rotor," *Experiments in Fluids*, Vol. 25, No. 4, 1998, pp. 352–361. doi:10.1007/s003480050240

[12] Mahaligam, R., and Komerath, N. M., "Characterization of the Near-Wake of a Helicopter Rotor," AIAA Paper 98-2909, 1998.

[13] Heineck, J. T., Yamauchi, G. K., Wadcock, A. J., and Lourenco, L., "Application of Three-Component PIV to a Hovering Rotor Wake," *56th Forum of the American Helicopter Society*, AHS International, Alexandria, VA, May 2000.

[14] Tangler, J. L., "Experimental Investigation of the Subwing Tip and Its Vortex Structure," NASA CR-3058, 1978.

[15] Muller, R. H. G., "Winglets on Rotor Blades in Forward Flight: A Theoretical and Experimental Investigation," *Vertica*, Vol. 14, No. 1, 1990, pp. 31–46.

[16] Liu, Z., Russell, J. W., Sankar, L. N., and Hassan, A. A., "A Study of Rotor Tip Vortex Structure Alternation Techniques," *Journal of Aircraft*, Vol. 38, No. 3, 2001, pp. 473–477.

[17] Lee, L., and Lee, T., "Oscillating-Wing Tip Vortex with Passive Short-Span Trailing-Edge Strip," *Journal of Aircraft*, Vol. 43, No. 3, 2006, pp. 723–731.

[18] Hardin, J. C., and Lamkin, S. L., "Concepts for Reduction of Blade/Vortex Interaction Noise," *Journal of Aircraft*, Vol. 24, No. 2, 1987, pp. 120–125.

[19] Brooks, T. F., Booth, E. R., Jolly, J. R., Yeager, W. T., and Wilbur, M. L., "Reduction of Blade–Vortex Interaction Noise Through Higher Harmonic Pitch Control," *Journal of the American Helicopter Society*, Vol. 35, No. 1, 1990, pp. 86–91.

[20] Cheng, R. P., Theodore, C. R., and Celi, R., "Effects of 2/Rev Higher Harmonic Control on Rotor Performance," *56th Forum of the American Helicopter Society*, AHS International, Alexandria, VA, 2–4 May 2000, pp. 1–35.

[21] Yong, C., Zimcik, D. G., Wickramasinghe, V. K., and Nitzsche, F., "Development of the Smart Spring for Active Vibration Control of Helicopter Blades," *Journal of Intelligent Material Systems and Structures*, Vol. 15, No. 1, 2004, pp. 37–47. doi:10.1177/1045389X04039655

[22] Straub, F. K., "Development of a Piezoelectric Actuator for Trailing-Edge Flap Control of Full Scale Rotor Blades," *Smart Materials and Structures*, Vol. 10, No. 1, 2001, pp. 25–34. doi:10.1088/0964-1726/10/1/303

[23] Enenkl, B., Kloppel, V., Preibler, D., and Janker, P., "Full Scale Rotor with Piezoelectric Actuated Blade Flaps," *28th European Rotorcraft Forum*, Royal Aeronautical Society, London, 17–19 Sept. 2002, pp. 89.0–89.14.
[24] Panagakos, A., and Lee, T., "Tip Vortex Control via an Active Trailing-Edge Tab," *Journal of Aircraft*, Vol. 43, No. 4, 2006, pp. 1152–1158.
[25] Gerontakos, P., and Lee, T., "Active Trailing-Edge Flap Control of Oscillating-Wing Tip Vortex," *AIAA Journal*, Vol. 44, No. 11, 2006, pp. 2746–2754.
doi:10.2514/1.19776
[26] Lee, T., and Gerontakos, P., "Investigation of Flow over an Oscillating Airfoil," *Journal of Fluid Mechanics*, Vol. 512, Aug. 2004, pp. 313–341.

E. Gutmark
Associate Editor